MIT Libraries | DSpace@MIT

MIT Open Access Articles

Surface-Mediated Bone Tissue Morphogenesis from Tunable Nanolayered Implant Coatings

Massachusetts Institute of Technology

Surface-mediated bone tissue morphogenesis from tunable nanolayered implant coatings*

Nisarg J. Shah[1,2], **Md. Nasim Hyder**[1,2], **Joshua S. Moskowitz**[1], **Mohiuddin A. Quadir**[1,2], **Stephen W. Morton**[1,2], **Howard J. Seeherman**[3], **Robert F. Padera**[4,5], **Myron Spector**[4,6,7], and **Paula T. Hammond**[1,2,8,*]

[1]Department of Chemical Engineering, Massachusetts Institute of Technology, 77 Massachusetts Ave., Cambridge, MA 02139, USA

[2]The David H. Koch Institute for Integrative Cancer Research, Massachusetts Institute of Technology, 77 Massachusetts Ave., Cambridge, MA 02139, USA

[3]Restituo LLC., 46 Trowbridge St., Cambridge, MA 02138, USA

[4]Harvard-MIT Division of Health Sciences and Technology, Massachusetts Institute of Technology, 77 Massachusetts Ave., Cambridge, MA 02139, USA

[5]Department of Pathology, Brigham and Women's Hospital, 75 Francis St., Boston, MA 02215, USA

[6]Tissue Engineering Laboratories, VA Boston Healthcare System, Mail Stop 151, 150 S. Huntington Ave., Boston, MA 02130, USA

[7]Department of Orthopedic Surgery, Brigham & Women's Hospital and Harvard Medical School, 75 Francis St., Boston, MA 02115, USA

[8]Institute for Soldier Nanotechnologies, Massachusetts Institute of Technology, 500 Technology Square, Cambridge, MA 02139, USA

Abstract

The functional success of a biomedical implant critically depends on its stable bonding with the host tissue. Aseptic implant loosening accounts for over half of all joint replacement failures. Various materials, including metals and plastic, confer mechanical integrity to the device, but often these materials are not suitable for direct integration with the host tissue, which leads to

---

implant loosening and patient morbidity. We describe a self-assembled, osteogenic, polymer-based conformal coating that promotes stable mechanical fixation of an implant in a surrogate rodent model. A single modular, polymer-based multilayered coating was deposited using a water-based layer-by-layer approach, by which each element was introduced on the surface in nanoscale layers. Osteoconductive hydroxyapatite (HAP) and osteoinductive bone morphogenetic protein 2 (BMP-2) contained within the nanostructured coating acted synergistically to induce osteoblastic differentiation of endogenous progenitor cells within the bone marrow, without indications of a foreign body response. The tuned release of BMP-2, controlled by a hydrolytically degradable poly(β-amino ester), was essential for tissue regeneration and, in the presence of HAP, the modular coating encouraged the direct deposition of highly cohesive trabecular bone on the implant surface. The bone-implant interfacial tensile strength was significantly higher than standard bone cement, did not fracture at the interface, and had long-term stability. Collectively, these results suggest that the multilayered coating system promotes biological fixation of orthopedic and dental implants to improve surgical outcomes by preventing loosening and premature failure.

INTRODUCTION

Implantable devices and scaffolds can replace damaged tissues, restore function, improve mobility, and alleviate pain. A major clinical issue that limits the success of orthopedic implants is failure owing to aseptic loosening and sub-optimal integration with the host tissue, which constitutes more than half of all joint replacement failures (1, 2). Implant loosening prolongs patient recovery times and increases post-operative complications and morbidity. The principal determinants of implant success are the nature and integrity of the bond between the implant and the bone, the rate at which the bond forms, and the amount of bone surrounding the implant that participates in stabilizing the device. Rapid, early stabilization of an implant by bone, without the formation of an avascular, loose fibrous tissue capsule are key determinants of long term implant function and integrity. Creating a mechanically competent, stable, permanent bond between implant and host bone through direct bone/implant contact is crucial for the success of dental implants and whole-joint replacement prosthesis.

Although widely accepted as the technique of choice for cemented hip and knee replacement implants, self-curing poly(methyl methacrylate) (PMMA)–based bone cements do not facilitate the formation of a reliable and mechanically coupled implant–bone bond owing to a substantial elastic modulus mismatch at the bone interface. PMMA has low compressive strength (70 – 120 MPa), is not bioresorbable, and is prone to fragmentation (3). Furthermore, the in situ formation of PMMA is a highly exothermic process that causes local tissue necrosis and makes it unfavorable for the incorporation and release of biologics that mediate the interaction between the host and implant. Other strategies to bond uncemented implants with the native bone have involved porous metallic coatings that have been clinically proven to induce bone ingrowth. However, this approach has been largely abandoned in knee implants owing to inadequate bone ingrowth and mechanical fixation (4).

Coatings that incorporate osteoconductive bioceramics, such as hydroxyapatite (HAP), have been used in the clinic for osseointegration of dental and orthopedic implants. However, plasma-deposited HAP coatings are several microns thick, have low tensile (45 – 65 MPa) and shear (25 – 40 MPa) strengths, are typically monolithic with invariant structural or mechanical properties, and have inadequate stress relief, which often results in cracks, rapid wear, and long-term instability within the body (5, 6). Consequently, failures associated with current HAP-based coatings occur at the implant-bone interface. High temperatures and grit blasting with high mechanical force have been used for the deposition of nanoscale HAP (7). However, this process is unfavorable for the incorporation of biologics. Modification of implant surfaces with cell adhesion molecules is inherently challenging owing to low selectivity across a variety of cell types, which can result in nonspecific attachment. These systems also lack tunable control over how long they are able to actively provide biochemical cues (8).

One of the proven bone differentiation factors currently employed in the clinic is bone morphogenetic protein 2 (BMP-2). The promise of this growth factor for bone tissue engineering depends critically on its delivery strategy (9, 10). Bolus release of BMP-2 from injectable or implantable carriers or depots results in a rapid clearance of the protein from the target site by serum proteins. Large quantities of recombinant human BMP-2 (rhBMP-2) —sometimes several orders of magnitude higher than needed—have been used in the clinic to compensate for suboptimal BMP-2 release characteristics of the carrier (11). The result was a lowered impact on tissue regeneration and undesired side effects (12). Hydrogel-based delivery systems can control the rate of release, but these systems deform easily and are unsuitable for imparting strong adhesion and mediating surface interactions on a permanent prosthesis.

We addressed these issues by coating implants using a layer-by-layer (LbL) technique (13-15). The polymer coatings (< 2 μm thick) consisted of osteoconductive base layers with HAP and osteoinductive BMP-2-releasing layers (16). The layered approach enabled tunable release of therapeutic levels of BMP-2 while providing an osteoconductive matrix for direct adhesion of osteoblasts. This thin multilayer coating conformed to implant geometries and recruited endogenous progenitor cells to form bone directly on the implant surface that integrated with the host cortical bone. The cohesive bone–implant interface resulted in the bonding and long-term stable fixation of the implant in vivo with rodent host tissue.

RESULTS

A two-part multilayer osteogenic coating

The base coating of the multicomponent film consisted of a set of permanent osteoconductive layers composed of a positively charged complex of cationic chitosan (Chi) (Fig. 1A) and HAP (Fig. 1B), alternated with anionic poly(acrylic acid) (PAA) (Fig. 1C) to form bilayers, indicated as [Chi(HAP)/PAA]$_X$ (where X is the number of bilayers). The mechanical properties of the film were examined using nanoindentation and revealed an elastic modulus of 11.39 ± 0.3 GPa (SEM) (fig. S1A). The elastic modulus dropped to 5.98 ± 0.32 GPa (SEM) in Chi/PAA polymer films without HAP.

The second component of the multilayer coating consisted of a polycationic degradable poly(β-amino ester), Poly2 (Fig. 1D). Poly2 was alternated with anionic PAA and positively charged rhBMP-2 (Fig. 1E) to generate a set of hydrolytically degradable layers atop the osteoconductive base (Fig. 1F) in the form of tetralayers, written as [Poly2/PAA/rhBMP-2/PAA]$_Y$ (where Y is the number of tetralayers). Under the acidic pH conditions of film fabrication, Poly2 was stable and the amines along its backbone were protonated, yielding a positive charge for electrostatic LbL assembly. The repeat unit for the osteoconductive base layers [Chi(HAP)/PAA]$_X$ and that of the growth factor–releasing layer [Poly2/PAA/rhBMP-2/PAA]$_Y$ are referred to as X and Y, respectively, and subscripted by the number of iterations.

Growth factor loading increased linearly with the number of layers, as observed in vitro for degradable LbL-coated PEEK and titanium implants with three different amounts of rhBMP-2 (fig. S1B). The total rhBMP-2 dose varied from 104.4 ± 16.8 (SEM) ng/mm^2 for the $X_{20} + Y_{20}$ coating (or Y_{20} alone) to 301.3 ± 17.2 (SEM) ng/mm^2 for the $X_{20} + Y_{60}$ (or Y_{60} alone) growth factor–loaded films (Fig. 1G). At pH 7.4, hydrolysis of the ester bonds in the exposed Poly2 chains resulted in the first-order in vitro release of rhBMP-2 from the LbL coating which lasted up to 15 days in cell culture media. All loaded rhBMP-2 eluted from the film, and none remained bound to the osteoconductive base layer. LbL coatings with extended incubation in rhBMP-2 solution had a higher total loading (than ng/mm^2 values seen for the rhBMP-2 deposited coatings): 1.8 μg/mm^2 for the X_{20} base layer and 2.9 μg/mm^2 with the 60 bilayer repeat [Poly2/PAA] coating. The osteoconductive base layer was designed to be permanent and maintained the same thickness on the substrate even after the release of growth factors (fig. S1C).

In all of the controlled-release layer formulations, $90 \pm 1.1\%$ (SEM) of rhBMP-2 eluted by 1 week. The average rate of release per day was $12.7 \pm 0.1\%$ (SEM) of total load with no burst release. rhBMP-2 retained bioactivity in vitro after release (fig. S2). Release profiles in vitro did not depend on implant geometry (Fig. 1G). By comparison, >90% of the therapeutic eluted within 24 hours of bolus release when the LbL films were loaded by extended incubation in rhBMP-2 solution.

To determine the physiological effect of these films, human mesenchymal stem cells (hMSCs) were cultured on the coated substrates and assayed for osteogenic differentiation via alizarin red. No calcium deposits were observed on uncoated substrates in growth media (Fig. 1H). Cells on uncoated substrates in differentiation media exhibited osteogenic differentiation and this average absorbance value (OD$_{600}$) was used to normalize all the experimental groups. The amount of calcium deposition did not improve beyond X_{20} in growth medium and was selected for further in vivo evaluation. The differentiation assay with X_{20} and varying numbers of rhBMP-2–releasing layers (Y) revealed a dose-dependent effect on calcium production. The results from X_{20} with extended incubation in rhBMP-2 solution were not significant compared to the X_{20} alone ($P = 0.19$, n = 9, Student's t test) and the effect of the biologic was not observed. The degradable [Poly2/PAA]$_{60}$ incubated for an extended time in rhBMP-2 was not significant from the uncoated control in growth media ($P = 0.17$, n = 9, Student's t test). This observation is consistent with rapid elution of growth factor and clearance after periodic changes of cell culture media.

Surface-mediated rhBMP-2 delivery

Implant integration and improvement of the rate and quality of tissue repair are the ultimate goals for biomaterial-based therapeutic strategies. To this end, we examined the effects of different combinations of the coating on poly(ether ether ketone) (PEEK) implants and medical-grade titanium implants that were either smooth or had 150-μm diameter channels drilled into the surface (table S1). Radiolucent PEEK permitted the use of radiography to monitor bone regeneration in real-time. The titanium implant model is a surrogate for dental and orthopedic clinical procedures in which the mechanical and biological integration of the implant with the surrounding bone is critical to its stability. In the clinic, porous implants are designed to enable adhesion interlock with bone and to increase the surface area for bone integration. In this study, each implant was press-fit into a circular unicortical defect drilled into the proximal tibia of a rat.

A near-IR fluorescent reporter was used to label rhBMP-2 and track its presence at the implant site over time in rodents (Fig. 2A). When rhBMP-2 release was controlled, the fluorescent signal at the implant site decreased over the course of 30 days. The gradual decline suggests that protein was retained within the peri-implant space, rather than being rapidly cleared by the local vascular transport systems. A pseudo–zero order regime was observed in vivocompared to the first-order release observed in vitro (Fig. 1G). Although in vivo rhBMP-2 release is primarily driven by hydrolytic degradation of the multilayers and would therefore be first-order, diffusion may play a role and the confined space at the implant site is a smaller sink than the highly dilute buffer solution used for *in vitro* measurements. LbL coatings on the implant subject to extended incubation in rhBMP-2 solution exhibited a burst release in vivo that was 3 orders of magnitude higher than the controlled release system and the profile was independent of the coating composition (Fig. 2B). The released rhBMP-2 was rapidly cleared in vivo, as measured by fluorescence, and was not detectable at the implant site 4 days after implantation.

These observations correlated with rhBMP-2 detected in homogenized bone marrow isolated from the tibia. rhBMP-2 was detected in the bone marrow aspirates of animals with both drilled and smooth implants in a dose-dependent manner (Fig. 2B). A peak in the dosage profile was detected several days after implantation of smooth PEEK implants followed by a subsequent monotonic reduction in rhBMP-2 that lasted for up to 4 weeks after implantation. Growth factor release from PEEK implants with drilled holes persisted over the same time scale as the smooth implants; however, instead of a defined peak, we observed a consistently high concentration over an extended multi-day period. This suggests that higher cumulative exposure to rhBMP-2 may be available at the drilled implant site for a prolonged period of times, owing to the sequestration of additional protein-loaded film within the channels.

In vitro release studies and a mass balance of total drug load in vivo revealed that the drilled implants had a higher drug load that correlated to the increase in total surface area of the drilled (20.26 mm^2) over the smooth (17.60 mm^2) implants (table S2). The effect of geometry on dosing in vivo was also observed with LbL coatings on implants incubated for an extended time in rhBMP-2 (Fig. 2B; fig. S3). Decreases in fluorescent signal correlated

with a drop in detectable levels of rhBMP-2 by ELISA, which suggested clearance of the growth factor from the implant site rather than degradation of the fluorophore.

Fluorescence-activated cell sorting (FACS) analysis on mesenchymal stem cells from the marrow revealed an increase in the osteoblast cell population ($CD29^+CD44^+CD45^-CD90^+BMPR1/2^+$) at 1 week, which was 3-fold greater in the $X_{20} + Y_{60}$ coating compared to X_{20} and Y_{60} alone, and 1.5-fold greater than $X_{20} + Y_{20}$ and $X_{20} + Y_{40}$ (Fig. 3; fig. S4). The percentage of osteoblast cells in the total cell population plateaued between week 4 and week 6 (Fig. 3), suggesting that a higher dose is beneficial primarily for the initial upregulation of the osteoblast population. This plateauing marks the end of the bone deposition process and the beginning of homeostasis. The pattern of cell activation on drilled implants was indistinguishable from smooth implant coatings at the same time point (Fig. 3) ($P > 0.2$, $n = 5$, Student's t test).

Integration of the implant with the bone tissue

Mechanical pull-out testing of the bone–implant interface was used to quantify the anchoring of the implant with bone. In this model of implant integration, the interfacial tensile strength was derived from bone adhesion to the implant surface and the connections that were made with the native bone tissue. The pull-out force increased over time in all groups with the LbL coatings for all types of implants (Fig. 4; fig. S5). The pull-out force was significantly higher in all implants coated with a combination of X and Y, compared to uncoated and to X_{20} or Y_{60} alone implants, including those incubated for an extended time in rhBMP-2 up to 4 weeks after surgery ($P < 0.05$, n = 5 implants per group time point, ANOVA with a Tukey post hoc test).

We investigated bone ingrowth into coated PEEK implants with smooth surfaces versus drilled holes (150 µm diameter). This size has been reported to encourage osteoid formation, and the ingrowth of mineralized bone (*17*). We observed a maximum pull-out force of 65.5 $\pm$ 1.3 N (SEM) following 4 weeks with the $X_{20} + Y_{60}$ coating on drilled implants and 39.7 $\pm$ 1.6 N (SEM) on smooth implants (Fig. 4). At 4 weeks, the pull-out force was found to be at least 2-fold higher when implants were coated with a combination of both X and Y coatings than implants with either the X_{20} or Y_{60} coating alone, and 32-fold higher than uncoated systems for both implant geometries. The pull-out force at 4 weeks was independent of rhBMP-2 dose. The same trends in pull-out force were observed with coated medical-grade titanium implants as with the PEEK implants. We observed a maximum pull-out force of 64.7 $\pm$ 2.2 N (SEM) following 4 weeks with the $X_{20} + Y_{60}$ coating on drilled implants and 41.1 $\pm$ 2.2 N (SEM) on smooth implants (fig. S6). The pull-out force at 4 weeks appeared to be independent of the implant material.

The pull-out force remained unchanged from 4 weeks to 18 months in groups with uncoated or Y_{60} coated PEEK implants. (Fig. 4). At this time point, the pull-out force of implants coated with the osteoconductive coating X_{20} was the same as the synergistic coating $X_{20} + Y_{60}$ ($P = 0.96$, n = 5, Student's t test), but the pull-out force of implants coated with just Y60 did not increase to match the other coatings thus confirming that HAP has a role in mediating formation of a mechanically competent interface. These data suggest that early bonding between bioactive materials and parent bone through the HAP layer is important to

bone tissue apposition and ingrowth. The interfacial tensile strength of coated implants, calculated by dividing the pull-out force by the implant surface area (table S3; table S4), with a combination of both X and Y was found to be 2- to 3-fold higher than HAP coatings on smooth implants using other methods of deposition (0.72-1.5 MPa) (18) and at least 3-fold higher than bioactive bone cements (0.07-0.9 MPa) in animals (19). While the LbL coatings maintain long-term strength over 18 months, a decrease in strength is observed other HAP coating methods over the same period (18). Burst-release rhBMP-2 does not have an effect on implant integration when it is introduced in LbL [Poly2/PAA]$_{60}$ films via a single post-coating extended incubation step in both drilled and smooth implants (Fig. 4; table S3; table S4).

Host-implant interactions at the cellular level

Histological sections of excised tibiae with intact PEEK implants with the dual $X_{20} + Y_{60}$ coating (Fig. 5) showed active bone formation and remodeling in time with activated, migrating osteoblasts forming cement lines (Fig. 5A). The new bone was laid down directly on the implants containing HAP in the coating, without a cartilaginous intermediate. We observed that the new bone progressively expanded outward to integrate with the surrounding parent bone. Consistent with stable bone adhesion, bone tissue was observed on the surface of implants that were pulled out of the tibiae, as the tensile tests resulted in cohesive fracture of bone rather than adhesive failure at the bone/implant interface (Fig. 5B). By comparison, for the osteoconductive base layer X_{20} alone, bone deposited on the surface of the PEEK implant with limited contact area, but connected with the host bone (fig. S7). When rhBMP-2 alone (Y_{60}) was introduced, the newly synthesized bone did not directly deposit on the implant surface (fig. S8).

In all coated implants, osteocytes were observed in the newly synthesized bone, indicating bone maturation (Fig. 5; fig. S7B; fig. S8B). Newly synthesized bone formation was restricted to the peri-implant space (Fig. 5A). The collagen fibrils in maturing new bone exhibited birefringence and were oriented along the implant surface (fig. S9A) and extended outward from the implant surface (fig. S9B). Hematopoietic cells were observed around areas of new trabecular bone (Fig. 5A), suggesting vascularization.

In implants containing drilled holes, mature bone formed within the implant pores coated with $X_{20} + Y_{60}$. Granulation tissue penetrated the channel and supplied progenitor cells that progressively filled in tissue from the periphery (Fig. 6, A and B). After 4 weeks, the entire channel filled with new bone (Fig. 6, C and D).

Fibrous tissue growth that is characteristic of a foreign body response was observed around implants without a coating (fig. S10, A and B), and did not convert into bone tissue after 4 weeks. This observation confirmed the lack of osseointegration with uncoated implants. There were no indications of adverse foreign body reactions in the animal in coated implants as evidenced by the lack of foreign body giant cells long-term inflammation or infection (Fig. 5).

Quantifying bone deposition

Micro-computed tomography (μCT) was used to image and quantify temporal bone volume and bone coverage in the peri-implant space (Fig. 7). Because the implant spanned the width of the medullary canal and protruded outside, bone was quantified at these regions of interest (ROIs). Within the medullary canal the ingrowth of bony tissue was observed and increased in volume and coverage over the course of 18 months for drilled and smooth implants coated with $X_{20} + Y_{60}$ (Fig. 7A). Interdigitation of the trabecular shell around the implant occurred at the cortical interface with the endosteal tissue. The volume and coverage of trabecular bone generally increased over time around coated implants (Fig. 7B). Limited calcification of the tissue was observed on implants coated with X_{20} layers alone. Greater calcification was observed with the Y_{60} coating alone.

The presence of rhBMP-2 by itself (Y_{60}) was not sufficient to induce bone apposition to the implant. In fact, the bone coverage/bone volume (BC/BV) around implants with the X_{20} coating was higher at 2 weeks than the Y60 coating alone. The BC/BV of new bone was significantly greater around implants coated with $X_{20} + Y_{20}$ or $X_{20} + Y_{60}$ than those coated with X_{20} or Y_{60} only over the course of 4 weeks. After 18 months, however, implants with the X_{20} coating had the same BC/BV as the combination $X_{20} + Y_{60}$. Nevertheless, bone coverage of the combination coatings reached > 90% in 2 weeks. Bone volume for the $X_{20} + Y_{60}$ surface coating increased from 113.5 ± 6.4 mm^3 (SEM) to 183.1 ± 9.0 mm^3 (SEM) between 2 and 4 weeks. Implants with surfaces coated with only X_{20} were slower to reach similar BC/BV, with < 50% coverage and only 75.1 ± 3.9 mm^3 (SEM) bone volume at 4 weeks.

On the periosteal side, no BV was observed around implants with the osteoinductive coating alone (Fig. 7C). Notably, the BC plateaued at 2 weeks post implantation, but the BV increased from 2 to 4 weeks for both X_{20} coated implants and implants coated with a combination of X and Y. This is consistent with the participation of progenitor cells from the periosteum in bone formation, on implants with the X_{20} layers. In all groups, no bone was observed to form a 'cap' around the implant on the periosteal side and resistance to tensile forces was entirely due to shear resistance of the new bone (Fig. 7A).

Similar observations were made for the smooth implants as for the drilled implants (fig. S11). However, the volume of bone formed in the medullary canal was lower in smooth versus drilled across different coating groups, probably owing to the reduced total surface area from a lack of drilled channels. The difference was $12.3 \pm 2.1\%$ (SEM), corresponding to the 13.1% lower surface area in smooth implants.

DISCUSSION

Worldwide revision rates for hip and knee prosthesis are about 12% after ten years and over half of all failures are due to aseptic loosening (1). Revision surgeries are burdensome on the patient, increase recovery times and often permanently restrict mobility. For knee revisions alone, the projected hospital costs may exceed $2 billion by 2030 (20). Revision surgeries stretch healthcare resources and result in significant financial losses in the system. This

burden, coupled with a projected increase in demand for hip, knee and dental implants is a significant driving force for the attenuation of premature implant failures.

In this study we have used a rational materials approach to rapidly induce implant fixation via a coating, using a programmable layer-by-layer technique. Chitosan (deacetylated chitin) is a linear cationic polysaccharide which is a hemostatic, antibacterial material, induces minimal foreign body reaction when used in composite scaffolds for bone regeneration, and contributes to the mechanical properties of the osteoconductive base layers (21). It is hydrolytically stable, and films made of chitosan have been demonstrated to be stable over several months (22). PAA is a well-characterized weak polyanion with a high charge density with a non-erodible backbone that has been listed as an approved excipient in the FDA's Inactive Ingredient Guide and is used in the clinic. LbL coatings span a wide range of elastic moduli (100 MPa – 20 GPa) (23). In this study, the elastic modulus of the osteoconductive base layer mimicked that of trabecular bone (~11 GPa) (24). This allowed for creating a graded transition between an implant and the host bone, thus eliminating mechanical mismatch.

The success of the LbL growth factor delivery strategy requires a polyion with a suitably low degradation rate. In this application, the use of a hydrolytically degradable polyion within the release films was key, as it enabled degradation independent of the presence of specific enzymes or cell types; furthermore, the release rate, critical for optimal tissue response, was readily tuned by the selection of the polymer. Poly2 is a synthetic polymer that belongs to the poly(β-amino ester) family of polymers, which have been used in gene delivery applications and deliver therapeutic payloads without cytotoxicity (25-27).

In prior LbL work, the substrate was coated with the polymer layers alone and then incubated in a concentrated solution of rhBMP-2 for an extended time (28, 29). In vivo, these systems induce bone formation. Typically, such systems exhibit a burst release profile, in which much of the therapeutic is ejected from the LbL coatings very quickly (>80% in less than 24 hours). We also observed this behavior in the implants incubated for an extended time in rhBMP- 2, where more than 90% of the biologic was eluted after 24 hours. This behavior is akin to known clinical bulk collagen carriers and depots in which 40 – 60% of the encapsulated protein is immediately released in the first three hours with low therapeutic effect (11, 30). The consequence of such release behavior in this study was none to suboptimal integration, in which the effect of rhBMP-2 is not observed. In addition, the LbL films described in this study are inherently osteoconductive due to the presence of HAP and can be deposited on virtually any bone implant material which may not be osteogenic.

HAP has been known to directly bind BMP-2 primarily via electrostatic interactions along with a number of other secondary interactions (31). However, HAP coatings that directly adsorb BMP-2 on hydroxyapatite lack the ability to load and release predictable amounts of growth factor (32). The release is purely diffusive and consequently dependent on loading concentration and environment conditions. The in vivo release kinetics of these systems is unclear, which has direct bearing on bone formation.

When the delivery is controlled, rhBMP-2 acting synergistically with HAP was more effective at mediating implant integration. The released rhBMP-2 bound to the bone matrix after gradual release was detectable with ELISA and in combination with a slow clearance rate from the implant site, an overall accumulation of BMP-2 was achieved. The observation of growth factor retention is consistent with similar observations of delivered therapeutic molecules in other systems (33). Additional factors that may have contributed to rhBMP-2 accumulation include lower hydrolysis rate due to the adsorption of proteins and shifts in pH in the wound healing environment at the implant site.

The dose of rhBMP-2 is essential successful osseointegration of implants, but current carriers lack dose tunability (34, 35). The coatings described here combine the advantages of synthetic materials with key biologics that regulate bone tissue development. Each component of the system can be reproducibly synthesized by chemical means with no risk of disease transmission, which compares favorably to the current clinical standard of bovine-derived absorbable collagen sponge. The coating architecture can be tailored by altering the total number of layers or by tuning the physical properties of the structural components. The mild, water-based coating scheme is adaptable and versatile. This system can be easily extended to incorporate and deliver several physiologically relevant growth factors together or in sequence.

It is important to note the limitations of the study as well as the remaining questions that warrant further investigation. First, the animal model, while standard for implant integration studies, is a surrogate for a joint or dental implant that would experience different dynamic loading conditions. Further evidence from pre-clinical investigations in large animals would be needed using joint and dental implants, as complex implant geometry and surface modification are both important for integration. Long-term superiority of the LbL system over more conventional rhBMP-2 loading strategies remains to be proven and has direct consequence to regulatory approval. The LbL coating may be best suited where there is a major clinical need, such as revision arthroplasty, where the implant has already failed, and primary joint replacements in osteoporotic patients, where there is a need to augment the lack of local bone. Second, although the LbL technique can coat a broad range of substrates —as we have demonstrated for both PEEK (plastic) and medical-grade titanium—and is extremely versatile, clinical manufacturing of dip- or spray-coated implants will require assembly in a sterile clean-room. The shelf-life of these implants would need to be determined. It is noted that some implant manufacturing companies have explored cyclic drop casting of rhBMP-2 on dental implants in a sterile environment (35). Orthogonally, methods for rapid high-throughput LbL coatings for non-medical applications are available (36). For a commercial implant LbL coating process, it may be necessary to harness the synergy of these processes as the ability to automate an efficient coating process in a sterile environment will be critical for feasible scale-up. Initially it may be advantageous to setup this process as stand-alone and subject to separate regulatory validation. Sufficient market demand could warrant integration with an existing implant manufacturing process and re-validation.

In summary, our study demonstrates that a tunable, programmed tissue engineering biointerface can integrate bone implants with the host tissue. Using osteoconductive

hydroxyapatite and osteoinductive rhBMP-2 incorporated into a single thin polymer implant coating, we demonstrated a serial effect of implant integration in a relevant rodent model. The results of this study suggest that a synthetic materials approach can be harnessed to access the osteogenic differentiation potential of endogenous precursor bone marrow stem cells and mediate specific, long-term host-tissue interactions. This approach provides a path to developing next-generation biologically integrated bone implants with superior stability, fewer incidences of failure and lower rates of patient morbidities.

MATERIALS AND METHODS

Rationale and study design

HAP and rhBMP-2 have been shown to benefit bone formation. We focused on evaluating tunable bone implant coatings containing these materials. The experiments compared the effect of their serial incorporation in multilayer implant coatings on bone integration. For animal studies, power analysis was conducted using GPower Analysis, using ANOVA repeated measures, between factors test. We assumed an effect size (f) of 0.5, an α error probability of 0.05, power of 0.95 and a correlation of 0.2. There were a total of 8 experimental groups with a at least 41 test animals per group. Each animal one implant in each leg (considered independent). Within each group, at least 5 implants were used for each measurement (IVIS, FACS, pull-out tensile testing and μCT) per time point. Some samples were used for representative histology. End-points were pre-determined to study the temporal effect of coatings of bone formation and implant integration. All experiments were randomized and non-blinded.

Preparation of electrostatic films

Poly2 (M_n = 11,910) was synthesized as described (25) and confirmed by NMR (fig. S12). Materials were purchased from Sigma unless otherwise noted. Sodium acetate buffer (0.1M, pH 4.0) was used for preparing polyelectrolyte solutions. Multilayer coatings were made using the LbL method (13-15). HAP nanoparticle suspension in buffer (0.1% w/v) was sterile-filtered and added 1:1 (v/v) to chitosan solution in buffer (2 mg/ml). Polyelectrolyte solutions were prepared at 1 mg/ml (PAA, Poly2). Dipping solutions were prepared at 250 μg/ml rhBMP-2 (Pfizer). Detailed LbL film fabrication and characterization is described in Supplementary Methods.

PEEK (McMaster-Carr) and titanium dowels (Titanium Industries) were machined into implants. These were plasma treated with air for 10 and 2 minutes, respectively, and alternatively dipped for 5 minutes each, into the prepared solutions with an intermediate washing step in water. The osteoconductive base layers (X) were deposited first followed by the osteoinductive layers (Y). X_{20}, or 60 bilayers of Poly2/PAA were incubated in a 250 μg/ml solution of rhBMP-2 at 4°C overnight.

Animal studies

All animal procedures were approved by the IACUC at MIT. Implants were inserted below the patella ligament in both the tibiae of adult male Sprague-Dawley rats. The implant

(diameter 1.3 mm) was inserted in a drilled hole (diameter 1.4 mm). Details in Supplementary Methods.

Pull-out tensile testing

After euthanasia, tibiae were explanted and stored in PBS for immediate mechanical tensile testing (Instron 5943). The exposed head of the implant was connected to a load cell and was then subjected to a constant pull rate of 0.1 N/s. The pull-out force, parallel to the long axis of implant, was the maximum load achieved before implant detachment due to failure. Interfacial shear strength was calculated by dividing the pull-out force by the total surface area of the implant.

Histology

After euthanasia, tibiae were explanted and were fixed in 4% paraformaldehyde (PFA). PFA-fixed tibiae with implants were partially decalcified for about 4 hours using a rapid decalcifying formic acid/hydrochloric acid mixture (Decalcifying Solution, VWR) and embedded in paraffin wax. Sections (5 μm) of the bone/implant interface were stained with routine hematoxylin and eosin (H&E) and Masson's trichrome stain. Implants were embedded in glycol methacrylate (JB-4 Plus, Polysciences) following the manufacturer's protocol and sectioned.

μCT analysis

Anesthetized live animals were imaged with a μCT (eXplore CT120, GE Medical Systems). Scanning protocol: Shutter speed (325 s), 2×2 binning, 70 kV, 50 mA, 220 images, 0.877° increments, gain: 100 and offset: 20. Images were reconstructed and analyzed with MicroView (GE Healthcare). A threshold value and ROI was chosen by visual inspection of images (constant for all groups) and BC/BV was measured.

Statistical analysis

Prism 5 (GraphPad) was used for all analyses. Results are presented as means ± SEM. Time points are after implanting. Data were analyzed by ANOVA and comparisons were performed with a Tukey post hoc test (multiple groups) or a Student's t test (two groups). ANCOVA was used to analyze trends in temporal measurements. $P < 0.05$ was considered significant.

Supplementary Material

Refer to Web version on PubMed Central for supplementary material.

Acknowledgments

REFERENCES AND NOTES

1. Labek G, Thaler M, Janda W, Agreiter M, Stöckl B. Revision rates after total joint replacement: cumulative results from worldwide joint register datasets. J Bone Joint Surg Br. 2011; 93:293–297. [PubMed: 21357948]

2. Ulrich SD, Seyler TM, Bennett D, Delanois RE, Saleh KJ, Thongtrangan I, Kuskowski M, Cheng EY, Sharkey PF, Parvizi J. Total hip arthroplasties: What are the reasons for revision? Int Orthop. 2008; 32:597–604. [PubMed: 17443324]

3. Lewis G. Alternative acrylic bone cement formulations for cemented arthroplasties: Present status, key issues, and future prospects. J Biomed Mater Res Part B Appl Biomater. 2007; 84:301–319. [PubMed: 17588247]

4. Berger RA, Lyon JH, Jacobs JJ, Barden RM, Berkson EM, Sheinkop MB, Rosenberg AG, Galante JO. Problems with cementless total knee arthroplasty at 11 years followup. Clin Orthop Relat Res. 2001; 392:196–207. [PubMed: 11716383]

5. Sun L, Berndt CC, Gross KA, Kucuk A. Material fundamentals and clinical performance of plasma-sprayed hydroxyapatite coatings: a review. J Biomed Mater Res A. 2001; 58:570–592.

6. Zheng X, Huang M, Ding C. Bond strength of plasma-sprayed hydroxyapatite/Ti composite coatings. Biomaterials. 2000; 21:841–849. [PubMed: 10721753]

7. Meirelles L, Arvidsson A, Andersson M, Kjellin P, Albrektsson T, Wennerberg A. Nano hydroxyapatite structures influence early bone formation. J Biomed Mater Res A. 2008; 87:299–307. [PubMed: 18181110]

8. Puleo DA, Nanci A. Understanding and controlling the bone-implant interface. Biomaterials. 1999; 20:2311–2321. [PubMed: 10614937]

9. Martino MM, Tortelli F, Mochizuki M, Traub S, Ben-David D, Kuhn GA, Muller R, Livne E, Eming SA, Hubbell JA. Engineering the growth factor microenvironment with fibronectin domains to promote wound and bone tissue healing. Sci Transl Med. 2011; 3:100ra89.

10. Nakashima M, Reddi AH. The application of bone morphogenetic proteins to dental tissue engineering. Nat Biotechnol. 2003; 21:1025–1032. [PubMed: 12949568]

11. Pashuck ET, Stevens MM. Designing Regenerative Biomaterial Therapies for the Clinic. Sci Transl Med. 2012; 4:160sr4. [PubMed: 23152328]

12. Carragee EJ, Hurwitz EL, Weiner BK. A critical review of recombinant human bone morphogenetic protein-2 trials in spinal surgery: emerging safety concerns and lessons learned. Spine J. 2011; 11:471–491. [PubMed: 21729796]

13. Decher G. Fuzzy Nanoassemblies: Toward Layered Polymeric Multicomposites. Science. 1997; 277:1232–1237.

14. Boudou T, Crouzier T, Ren K, Blin G, Picart C. Multiple functionalities of polyelectrolyte multilayer films: new biomedical applications. Adv Mater. 2010; 22:441–467. [PubMed: 20217734]

15. Decher, G.; Schlenoff, JB. Multilayer Thin Films: Sequential Assembly of Nanocomposite Materials. Second Edition. New York: Wiley; 2012.

16. Shah NJ, Hong J, Hyder MN, Hammond PT. Osteophilic multilayer coatings for accelerated bone tissue growth. Adv Mater. 2012; 24:1445–1450. [PubMed: 22311551]

17. Petite H, Viateau V, Bensaid W, Meunier A, de Pollak C, Bourguignon M, Oudina K, Sedel L, Guillemin G. Tissue-engineered bone regeneration. Nat Biotechnol. 2000; 18:959–963. [PubMed: 10973216]

18. Hong L, Xu HC, de Groot K. Tensile strength of the interface between hydroxyapatite and bone. J Biomed Mater Res. 1992; 26:7–18. [PubMed: 1315777]

19. Skripitz R, Aspenberg P. Attachment of PMMA cement to bone: force measurements in rats. Biomaterials. 1999; 20:351–356. [PubMed: 10048407]

20. Lavernia C, Lee DJ, Hernandez VH. The increasing financial burden of knee revision surgery in the United States. Clin Orthop Relat Res. 2006; 446:221–226. [PubMed: 16672891]

21. Di Martino A, Sittinger M, Risbud MV. Chitosan: a versatile biopolymer for orthopaedic tissue-engineering. Biomaterials. 2005; 26:5983–5990. [PubMed: 15894370]

22. Ren D, Yi H, Wang W, Ma X. The enzymatic degradation and swelling properties of chitosan matrices with different degrees of N-acetylation. Carbohydr Res. 2005; 340:2403–2410. [PubMed: 16109386]

23. Tang Z, Wang Y, Podsiadlo P, Kotov NA. Biomedical Applications of Layer-by-Layer Assembly: From Biomimetics to Tissue Engineering. Adv Mater. 2006; 18:3203–3224.

24. Zysset PK, Guo XE, Hoffler CE, Moore KE, Goldstein SA. Elastic modulus and hardness of cortical and trabecular bone lamellae measured by nanoindentation in the human femur. J Biomech. 1999; 32:1005–1012. [PubMed: 10476838]

25. Lynn DM, Langer R. Degradable poly(beta-amino esters): Synthesis, characterization, and self-assembly with plasmid DNA. J Am Chem Soc. 2000; 122:10761–10768.

26. Shukla A, Fleming KE, Chuang HF, Chau TM, Loose CR, Stephanopoulos GN, Hammond PT. Controlling the release of peptide antimicrobial agents from surfaces. Biomaterials. 2010; 31:2348–2357. [PubMed: 20004967]

27. Shah NJ, Macdonald ML, Beben YM, Padera RF, Samuel RE, Hammond PT. Tunable dual growth factor delivery from polyelectrolyte multilayer films. Biomaterials. 2011; 32:6183–6193. [PubMed: 21645919]

28. Crouzier T, Sailhan F, Becquart P, Guillot R, Logeart-Avramoglou D, Picart C. The performance of BMP-2 loaded TCP/HAP porous ceramics with a polyelectrolyte multilayer film coating. Biomaterials. 2011; 32:7543–7554. [PubMed: 21783243]

29. Facca S, Cortez C, Mendoza-Palomares C, Messadeq N, Dierich A, Johnston AP, Mainard D, Voegel JC, Caruso F, Benkirane-Jessel N. Active multilayered capsules for in vivo bone formation. Proc Natl Acad Sci U S A. 2010; 107:3406–3411. [PubMed: 20160118]

30. Seeherman H, Wozney JM. Delivery of bone morphogenetic proteins for orthopedic tissue regeneration. Cytokine Growth Factor Rev. 2005; 16:329–345. [PubMed: 15936978]

31. Dong X, Wang Q, Wu T, Pan H. Understanding adsorption-desorption dynamics of BMP-2 on hydroxyapatite (001) surface. Biophys J. 2007; 93:750–759. [PubMed: 17617550]

32. Sachs A, Wagner A, Keller M, Wagner O, Wetzel WD, Layher F, Venbrocks RA, Hortschansky P, Pietraszczyk M, Wiederanders B, Hempel HJ, Bossert J, Horn J, Schmuck K, Mollenhauer J. Osteointegration of hydroxyapatite-titanium implants coated with nonglycosylated recombinant human bone morphogenetic protein-2 (BMP-2) in aged sheep. Bone. 2005; 37:699–710. [PubMed: 16139577]

33. Peters MC, Polverini PJ, Mooney DJ. Engineering vascular networks in porous polymer matrices. J Biomed Mater Res. 2002; 60:668–678. [PubMed: 11948526]

34. Reichert JC, Cipitria A, Epari DR, Saifzadeh S, Krishnakanth P, Berner A, Woodruff MA, Schell H, Mehta M, Schuetz MA, Duda GN, Hutmacher DW. A Tissue Engineering Solution for Segmental Defect Regeneration in Load-Bearing Long Bones. Sci Transl Med. 2012; 4:141ra93.

35. Wikesjö UM, Xiropaidis AV, Qahash M, Lim WH, Sorensen RG, Rohrer MD, Wozney JM, Hall J. Bone formation at recombinant human bone morphogenetic protein-2-coated titanium implants in the posterior mandible (Type II bone) in dogs. J Clin Periodontol. 2008; 35:985–991. [PubMed: 18976395]

36. Krogman KC, Lowery JL, Zacharia NS, Rutledge GC, Hammond PT. Spraying asymmetry into functional membranes layer-by-layer. Nat Mater. Apr.2009 8:512. [PubMed: 19377464]

37. Oliver WC, Pharr GM. Measurement of hardness and elastic modulus by instrumented indentation: Advances in understanding and refinements to methodology. J Mater Res. 2004; 19:3–20.

38. Gregory CA, Gunn WG, Peister A, Prockop DJ. An Alizarin red-based assay of mineralization by adherent cells in culture: comparison with cetylpyridinium chloride extraction. Anal Biochem. 2004; 329:77–84. [PubMed: 15136169]
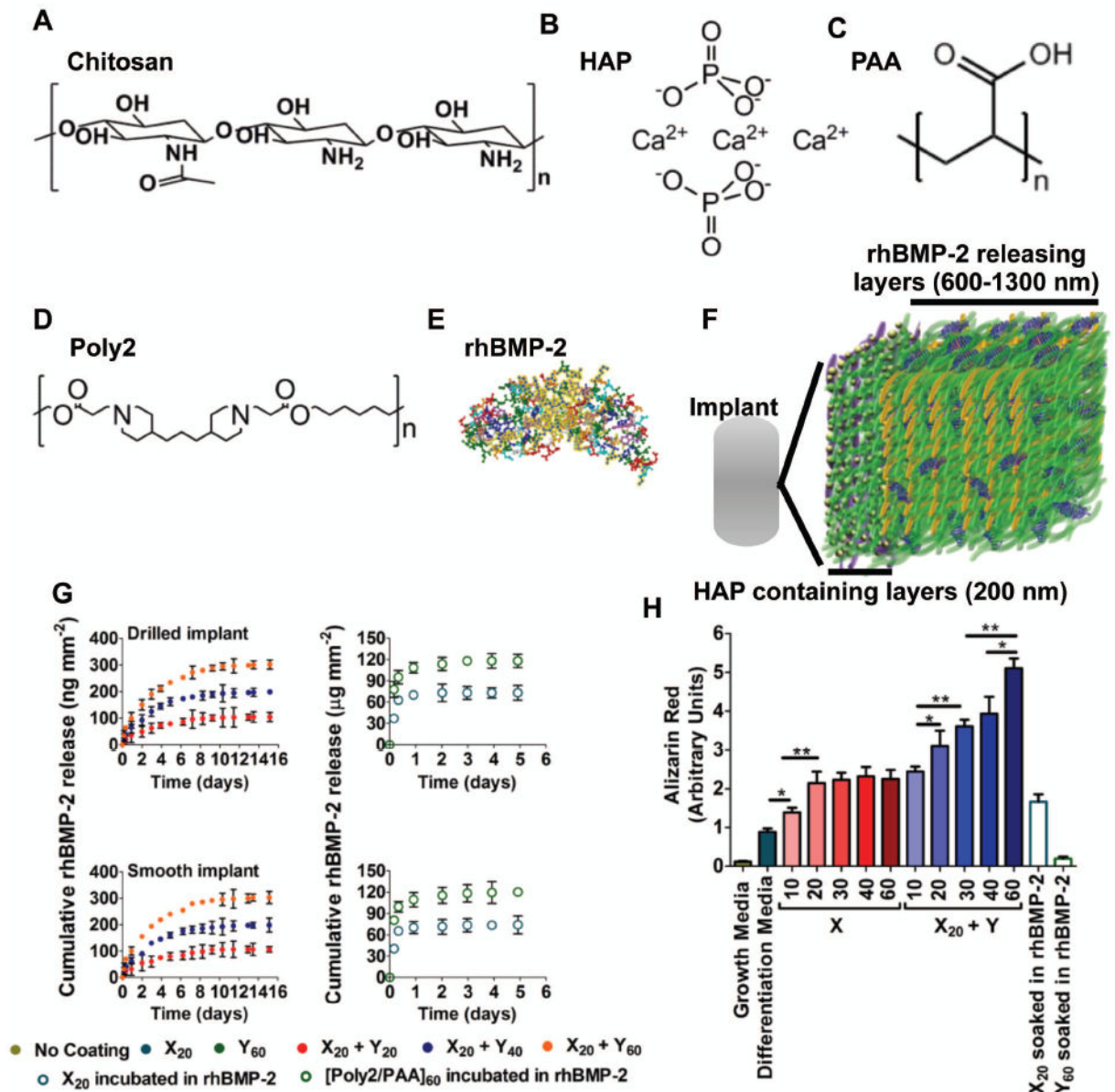
Figure 1. Structured coatings for bone regeneration are made up of two composite multilayers

(**A** to **C**) The base coating contains chitosan (Chi; 75-85% deacytelated chitin, $M_v \sim 100$ kDa) and hydroxyapatite [HAP; $Ca_{10}(PO_4)_6(OH)_2$] with poly(acrylic acid) (PAA; $M_v \sim 450$ kDa) in a bilayer repeat unit. (**D** and **E**) The osteogenic factor coating contains a hydrolytically degradable poly(β-amino ester) (Poly2, $M_v \sim 11$ kDa) and rhBMP-2 that are alternated with PAA on top of the osteoconductive base coating. (**F**) Schematic of the two sets of multilayers: osteoconductive and osteoinductive. (**G**) Cumulative release profile of rhBMP-2 from drilled implants. Data are means $\pm$ SEM ($n = 9$ per coating). (**H**) rhBMP-2 loading has a dose-dependent effect on calcium deposition, quantified by alizarin red at 14 days. Data are means $\pm$ SEM ($n = 6$-9). $* P < 0.05 ** P < 0.01$, ANOVA with a Tukey post hoc test.
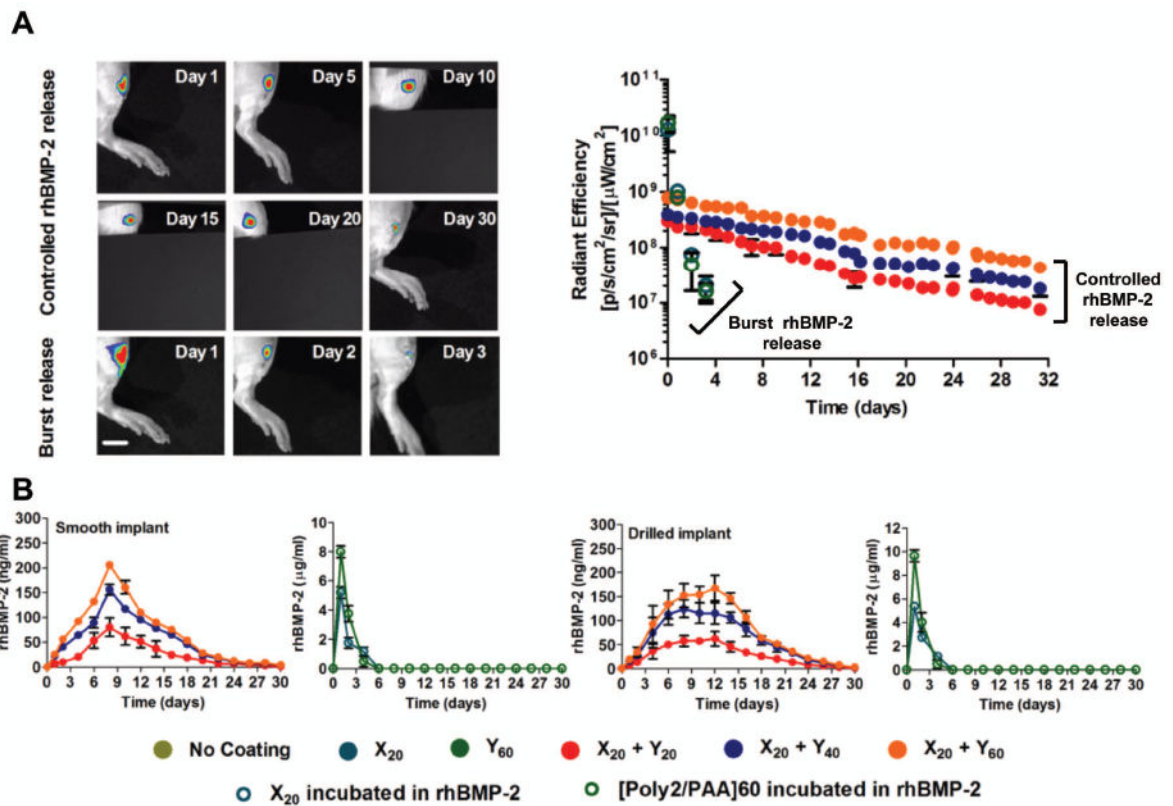
Figure 2. In vivo evaluation of rhBMP-2 release

rhBMP-2 was loaded into the multilayers that coated smooth and drilled PEEK rods and then implanted in the tibias of rats (n = 41-45 per group). (**A**) Controlled and burst release of fluorescently labeled rhBMP-2 was tracked in vivo over 30 and 3 days respectively. (**B**) Radiant efficiency at the implant site over time (n = 4-6 per group). (**C**) Bone marrow flushed out of excised tibiae was assayed for rhBMP-2 using ELISA for smooth and drilled implants. Data are means ± SEM (n = 5-6 per group).
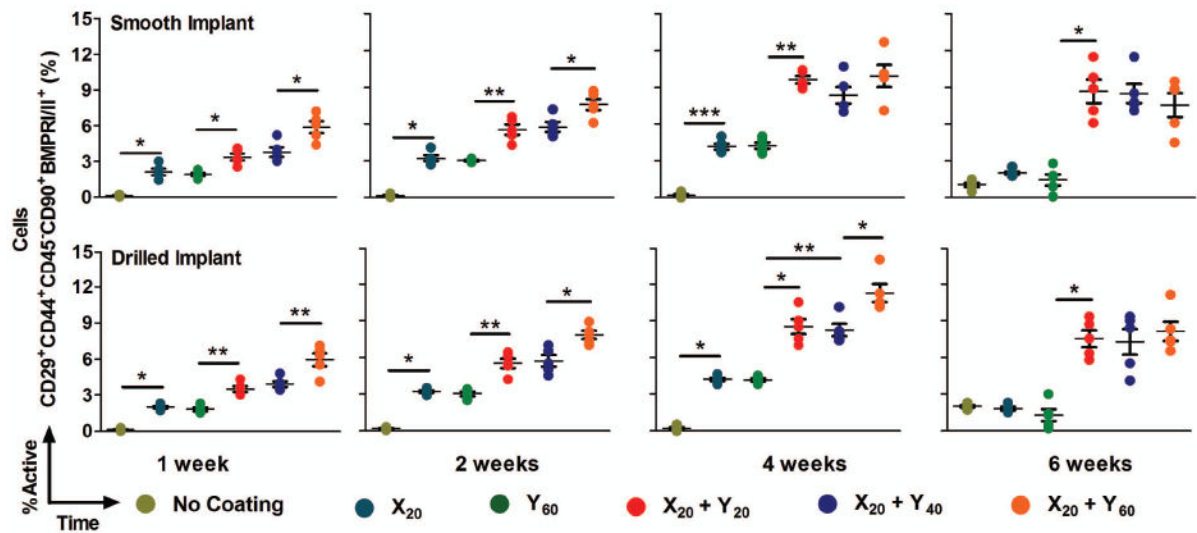
Figure 3. Mesenchymal stem cells differentiate into osteoblasts
Five color flow cytometry was used to assess the percentage of osteoblasts in cells isolated from the tibia marrow around smooth and drilled implants. Each point represents individual implants. Means ± SEM ($n = 5$ per group). *$P < 0.05$, **$P < 0.01$, ANOVA with a Tukey post hoc test. FACS plots are provided in fig. S4.
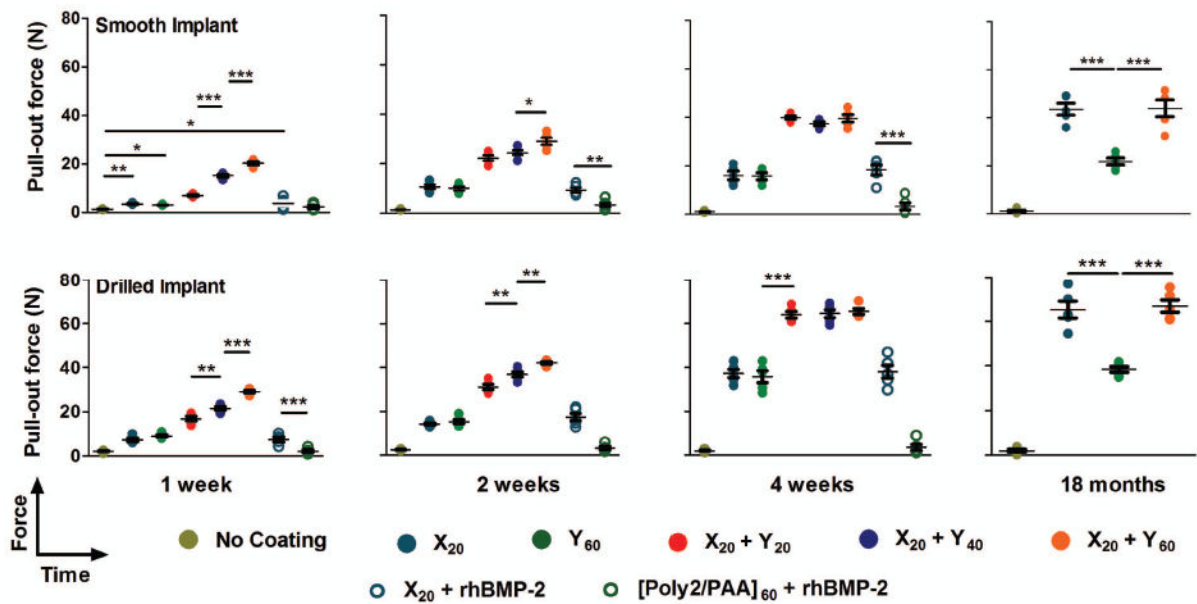
Figure 4. Tensile force testing of implants from the rat tibia

Force data from individual implants are presented from smooth and drilled implants. Data are means ± SEM ($n = 5$ implants per group time point). *p < 0.05; **p < 0.01; ***p < 0.001, ANOVA with a Tukey post hoc test. Interfacial tensile strength data are provided (table S1 and S2).
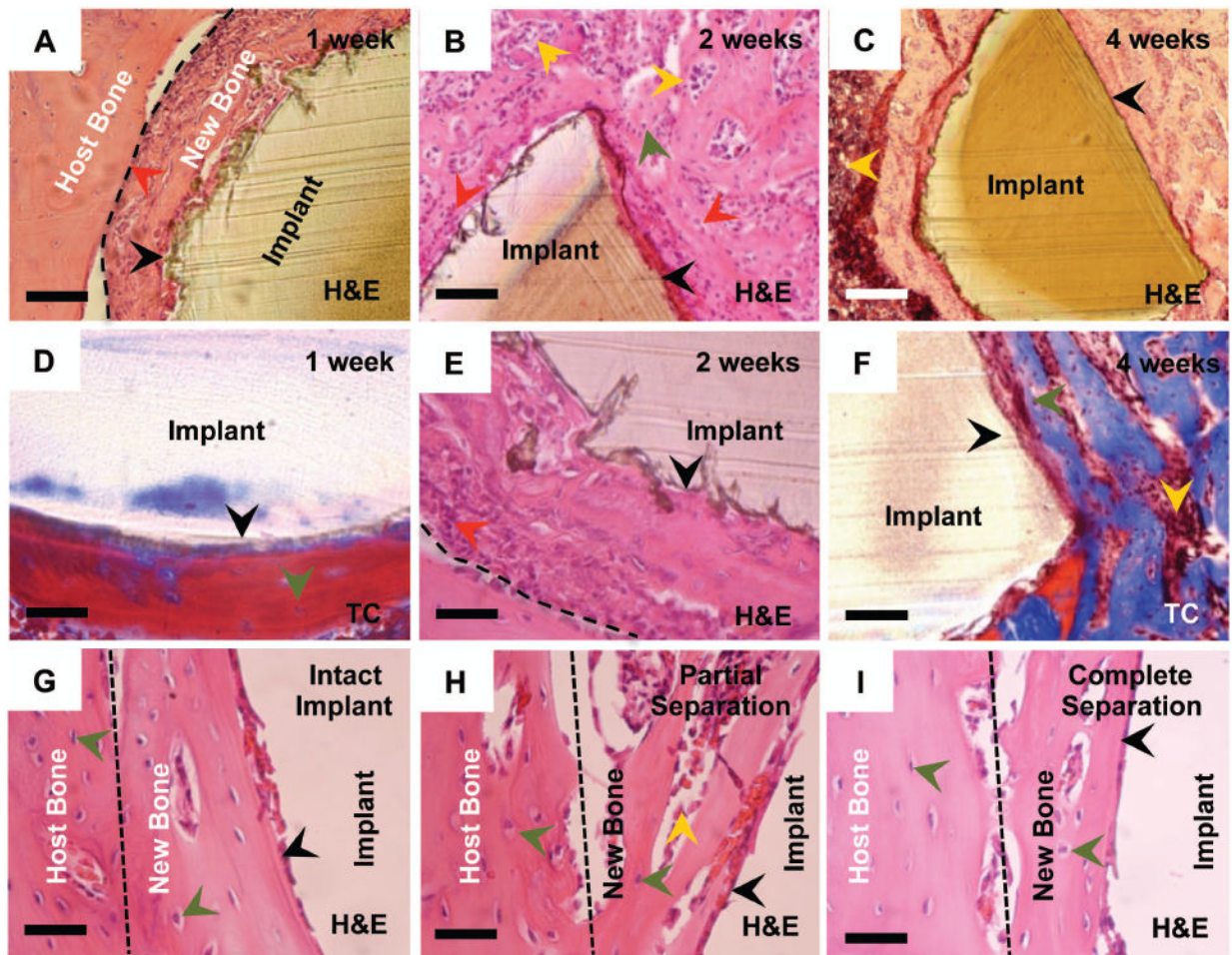
Figure 5. Histology of implants with various coating formulations demonstrating bone tissue morphogenesis at the implant interface
(**A** to **F**) Implants coated with $X_{20} + Y_{60}$ at 1, 2 and 4 weeks post-implantation demonstrating the process of implant integration with the parent bone tissue. Cement lines (broken black line) are observed on some sections. (G) The plane of fracture in implants with the $X_{20} + Y_{60}$ coating is indicated by a broken black line at 4 weeks which depict an intact implant, partial separation from the host bone and complete separation from the host bone. The new bone-implant interface is intact. Sections were viewed under bright field microscopy. Scale bars: (A and C) are 200 μm; (B) and (D to G) are 50 μm. Arrows: black, bone/implant interface; red, active osteoblasts; dark green, osteocytes; yellow, marrow cells. H&E: hematoxylin & eosin stain, TC: Masson's trichrome stain.
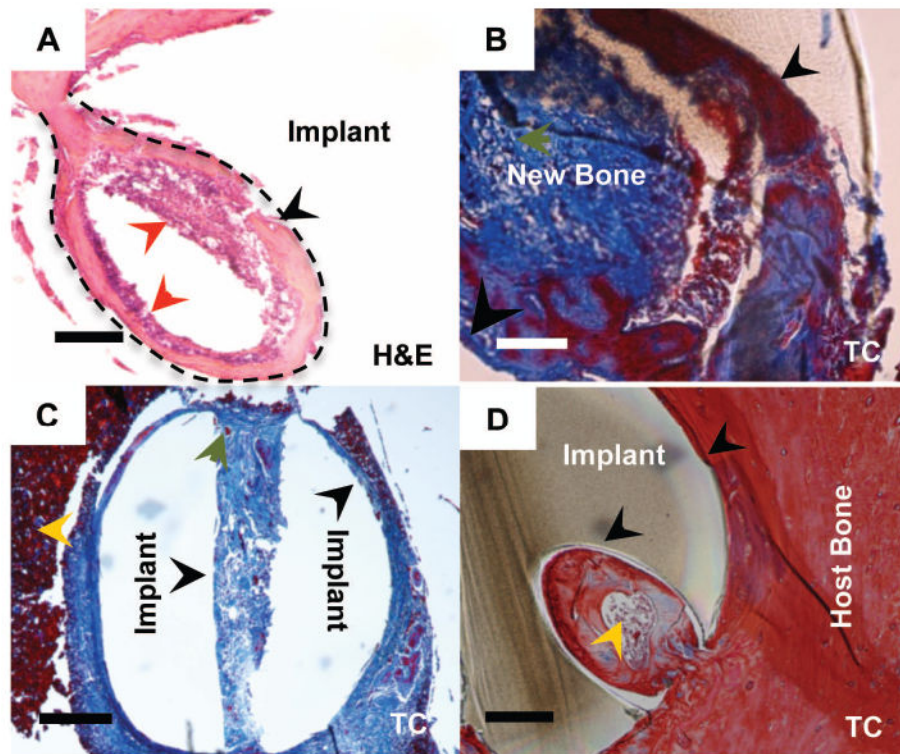
Figure 6. Bone deposition in the channels of drilled implants

Representative sections (n = 5-6 per group) of drilled implants after 4 weeks, which were coated with X_{20} + Y_{60}. (**A**) Granulation tissue (broken black line) penetrated the channel and supplied progenitor cells. (**B**) Newly deposited bone (blue) matures (red) and (**C**) gradually filled up the channel at 4 weeks. (**D**) Bone (blue and red) is present throughout the channel of a drilled implant. Sections were viewed under brightfield microscopy. Scale bars in (A, B and D) are 100μm and in (C) is 400 μm. Arrows: black, bone/implant interface; red, active osteoblasts; dark green, osteocytes; yellow, marrow cells. H&E: hematoxylin & eosin stain, TC: Masson's trichrome stain.
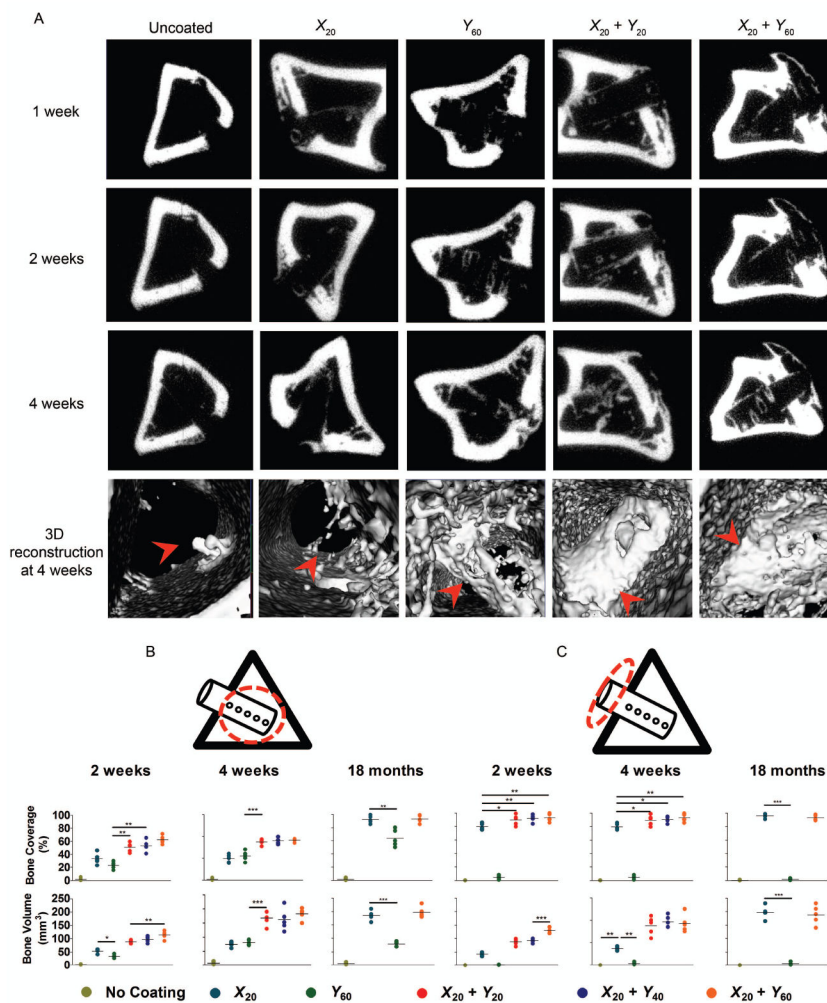
Figure 7. µCT imaging of bone formation on drilled PEEK implants

(**A**) Radiographs of bone formation around drilled implants with different coatings at 1, 2, and 4 weeks. Red arrows indicate location of the implant. (**B** and **C**) The images in (A) were used to quantify bone regeneration at 2 and at 4 weeks within (B) and outside the medullary canal (C) (using regions of interest marked by dotted red circles). Each point represents individual implants. Data are means ± SEM (n = 5-6 per group). *p < 0.05, **p < 0.01, ANOVA with Tukey post hoc test. Data for smooth implants are provided in fig. S11.